Received: June 17, 2023. Revised: September 16, 2023. 620

International Journal of
Intelligent Engineering & Systems

http://www.inass.org/

Early-stage Glaucoma Disease Prediction Using Ensemble Optimized Deep Learning Classifier Model

Jincy C Mathew[1]* V. Ilango[2] V Asha[1]

[1]*Department of MCA, New Horizon College of Engineering, Bengaluru, India*
[2]*Department of Computer Application, CMR Institute of Technology, Bengaluru, India*
[1,2]*Visvesveraya Technological University, Belagavi -590018, India*
* Corresponding author's Email: jincycm26@gmail.com

Abstract: Nowadays, retinal fundus images (RFI) play a crucial role in the early and exact prediction of glaucoma. Glaucoma is a vision-threatening eye illness that primarily impairs the eye nerves, and the serious condition of glaucoma leads to permanent vision loss. Several computer vision-based techniques have been explored in past studies for glaucoma detection, but those have certain misclassification results and are not much focused on early stage detection. This work presents an ensemble deep network (Ensemble DeepNet) model for the early detection of glaucoma via retinal fundus images. Initially, the kernel bilateral filter (kernel BF) is employed to improve the clarity of retinal images and reduces image noise. Then, the brightness of the input image is modified using linear histogram transformation (LHT). Further, the segmentation of the optic disc (OD) and optic cup (OC) is performed using two-stage thresholds U-network (Two-stage TUNet). Finally, a new ensemble DeepNet model is developed based on VGGNet, DenseNet, and CapsNet models using a weighted majority voting technique. The improved aquila optimization (IAO) algorithm is used to find the optimal weights for the ensemble DeepNet model. The proposed ensemble DeepNet model attains the highest of 99.45%, which shows that the proposed ensemble model is highly suitable for predicting glaucoma disease in an early stage.

Keywords: Optic disc, Optic cup, Two-stage threshold U-network, Kernel bilateral filter, Linear histogram transformation.

1. Introduction

Glaucoma is a permanent visual illness that affects the eyes and causes irretrievable blindness. It is one of the retinal disorders responsible for severe and persistent vision loss in people over 60 [1-2]. This disease is mainly caused due to excessive IOP (intraocular pressure) in the eye, which results in damaging the optic nerve [3]. Globally, this disease is called the thief of sight, the second leading disease. Over the year 2020, the ratio of affected people may likely rise from 79.6M (Million) [4]. Glaucoma is characterized based on the loss and malfunctioning of ganglion cells leading to changes in ONH (optic nerve head) structure, inner plexiform layers, and retinal nerve thickness [5].

The patient affected by glaucoma shows no initial symptoms in the advanced stage. Without proper treatment, glaucoma can cause severe damage to the optic nerve (ON) and thus lead to blindness [6, 7]. The diagnosis of glaucoma is performed by measuring the thickness of the cornea, manual optical disk (OD) examination, and monitoring of field vision and intraocular pressure. One of the most common methods of glaucoma diagnosis is the analysis of dilated pupils present in the eye by an ophthalmologist. However, the retinal analysis process done by ophthalmologists is tedious, manual, and time-consuming [8, 9]. Nowadays, computer vision-based models are utilized for early disease prediction. Therefore, early glaucoma diagnosis at the initial affected stages can effectively minimize the permanent risk of vision loss [10, 11].

Computer-aided diagnostics improve diagnosis time and aid in locating a specific location [12, 13]. Glaucoma refers to an eye disorder caused by extra

fluids in the eye it damages the visual nerve and causes blindness. Glaucoma is a different type, namely chronic or open-angle Glaucoma, NTG (normal-tension Glaucoma), acute angle-closure glaucoma, nonvascular glaucoma [14] etc. The main difficulty in identifying glaucoma is that it has no symptoms/pain, and eyesight is normal in the early stages. It is visible in the last stage after the patient has lost 70% of his vision. Regular eye screening is required in order to detect early glaucoma [15].

During the initial stages, ophthalmologists perform a physical eye grading by examining the OD area and CDR (cup-to-disc ratio) to identify abnormalities in border areas [16, 17]. But the diagnosis is often delayed due to fewer experts available, which has increased the number of affected people. Thus, automated detection methods have obtained major attention and have been applied in the medical image analysis field. DL is an ML subset that automatically extracts image attributes without requiring professional intervention [18-20]. With the technical advancements, the DL models have been built for various purposes, including image classification, event detection, object detection, medical image-based disease diagnosis, etc. The emergence of DL models can record fundus images and has shown possible improvements in evaluating the ONH via these fundus images, leading to an improved glaucoma diagnosis.

Contribution: The key contribution of the proposed work is listed below,

- To develop an ensemble deep network for the early-stage automated glaucoma prediction with the retinal fundus images.
- To perform two-stage threshold-based U-network segmentation of OD and OC in order to improve classification accuracy.
- To examine the various types of deep features from the retinal fundus images and to predict healthy and glaucomatous images with the ensemble optimized DL classifiers.
- The loss in the Ensemble DeepNet is optimized using the improved aquila optimization (IAO) algorithm.

The structure of this article is organized as follows: Section 2 reviews previous research on early-stage glaucoma illness prediction problems using various optimization methodologies. Kernel BF, LHT, image segmentation (OD and OC), two-stage threshold U-network, ensemble DeepNet, and IAO are all defined in section 3. The kernel BF and LHT used for image pre-processing improve and adjust the brightness. The OD and OC are segmented using a two-stage Threshold U-Network. Section 4 discusses the rim-one-dl and KGD dataset results. Normal and glaucoma images from the KGD and rim-one-dl datasets are shown visually. Ensemble DeepNet trains many networks on the same dataset and then predicts using each of the trained models before integrating the predictions in some fashion to get an outcome or prediction. Finally, IAO can help with weight loss. Section 5 experimental evaluation comprises mathematically developed system models for sensitivity, specificity, accuracy, and AUC. Section 6 concludes the paper.

2. Related works

Some of the research work related to glaucoma detection is:

Thakur and Juneja [21] presented the deep learning based early-stage glaucoma prediction, which minimizes the surgical need. The classification of glaucoma was employed with a CAD system and different DL classifiers such as VGG, Xception, ResNet, inception, and DenseNet for automatic diagnosis. The DL evaluation saves the patient's time and minimizes the cost and time of the diagnostic process. The datasets RIM-ONE and DRISHTI were merged and used as a single dataset for experimentation. The overall limitation identified was the excess time taken for training the network.

Singh et al. [22] developed an enhanced glaucoma diagnosis using the deep image model and feature extraction in fundus retina images. At first, pre-processing was performed with MF (median filter) along with image cropping and G-channel (green) extraction. Next, the segmentation of both OD and OC was done using the MSER (maximally stable external region) to localize the disc and separate the shell area from the entire disc region. Next, 20 diverse features were extracted and classified using different classifiers such as NB, KNN, ANN and SVM. The dataset used for testing was DRIONS-DB. The drawbacks were fewer metrics and a single dataset was considered for the evaluation.

Neto et al. [23] presented glaucoma screening in retinal images using DL approaches. The classification was done with different architectures, such as C2 (ResNet152 V2), C1 (Xception) and C3 (Inception ResNetV2). The activation maps of these models were analyzed, which can be further used to assist glaucoma predictions. The evaluation of glaucoma was done based on the CDR calculation done with the U-Net based DL architecture. The performance was experimented with by eliminating the last classification layer and adding 4 more layers

like 2d GAP (Global average pooling), dropout, BN (batch normalization), and Dense layer with Softmax activation. Three different datasets, such as REFUGE, RIM-ONE, and DRISHTI-GS, were used for experimentation. The accuracy of glaucoma prediction was higher (0.97) with the C1 model when tested with the REFUGE dataset. The drawback was that the analysis was only with binary classification.

Cho et al. [24] introduced the stage classification of glaucoma using the DL based ensemble method. The images were pre-processed to eliminate the black area around the edges. The augmentation procedure minimized the overfitting of image data. The input images were rotated at different angles and transformed into images of size $299 \times 299 \times 3$. Here, the convolutional neural network (CNN) model was used to perform the glaucoma stage classification, and the CNN parameters were optimized with different image filters. The glaucoma prediction was validated using four CNN models for improvising the accuracy. The grading of fundus images was measured with the average probabilities of every class. The glaucoma grading was categorized as C0 (unaffected control), C1 (early-stage glaucoma) and C2 (late-stage glaucoma). The dataset images have been collected from different hospitals. The limitations were higher FPR with unaffected control and higher mis-prediction with severity classification.

A deep learning-based CNN was proposed by Medeiros et al. [25] to evaluate the fundus photographs for assessing the spectral domain optical coherence tomography (SD OCT) global retinal nerve fibre layer (RNFL) thickness evaluations. The ability to recognize eyes with statistically important slopes of SD OCT variations was evaluated using receiver operating characteristic (ROC) curves. The main objective of this research work is to determine the association between the variation in projected RNFL thickness from photographs and the variation in SD-OCT RNFL thickness over time. The dataset utilized in this research was gathered from the duke glaucoma registry.

Jammal et al. [26] compared the capability of machine-to-machine procedures in order to predict the RNFL thickness evaluations from SD OCT. The process was done by utilizing a simple kind of color fundus photograph. A strong hypothesis was made that the SD OCT trained machine-to-machine prediction possessed a strong connection with visual field metrics compared to the subjective gradings performed by human specialists. In this research, a cross-sectional study was conducted using data from the duke glaucoma repository. The dataset holds information on comprehensive ophthalmologic validations during evaluations, medical history, etc. The error minimization and better specificity rate were the significant merits.

An effective algorithm was developed by Thakur et al. [27] to recognize glaucoma from a possible longitudinal study. The primary goal of estimating the accuracy of deep learning approaches is detecting the development of glaucoma from fundus images. Overall, 66,721 fundus images captured from 3272 eyes of over 1636 subjects contributed to the ocular hypertension treatment study (OHTS) were involved. Fundus images and pictorial fields were cautiously observed by two independent readers of the visual field and OD reading locations OHTS.

Sejong et al. [28] developed a machine learning prediction approach for effective glaucoma recognition. For the feature selection process, clinical information from patients based on visual field experiments, RNFL-OCT testing, joint validation with measurement of intraocular pressure (IOP) and fundus images was presented. The machine learning-based prediction approach was developed using five selected features, and the performance was analyzed with 10-fold cross-validation. Table 1 describes the analysis of glaucoma disease prediction with its respective merits and demerits.

Kumar et al. [29] implemented a glaucoma detection strategy based on a hybrid deep learning model with the heuristic technique. At first, contrast limited adaptive histogram equalization (CLAHE) method was applied to retinal fundus images for pre-processing. Then, the segmentation was done by U-shape network (Unet++) architecture for separating the disc and cup parts. Finally, the hybrid deep learning model of residual network (ResNet) with gated recurrent units (ResNet-GRU) was employed for glaucoma detection. Moreover, the modified density.

Factor-based honey badger algorithm (MDF-HBA) was used for optimizing the parameters of the deep learning model.

Nawaz et al. [30] presented a deep learning based framework based on the backbone of EfficientDet-D0 and EfficientNet-B0 models. Initially, the EfficientNet-B0 feature extractor was used to extract the deep features from the suspected fundus images. Further, the keypoints fusion was performed multiple times based on top-down and bottom-up manner using the bi-directional feature pyramid network (BiFPN) module of EfficientDet-D0 model. Finally, the localized region comprising glaucoma lesion with related classes was predicted.

Kashyap et al. [31] proposed a deep learning model to identify and predict the glaucoma class of fundus images correctly for early diagnosis. The optic cub region was segmented using the pre-trained

Table 1. Analysis of glaucoma disease prediction

Author name and Reference	Techniques used	Objective	Merits	Demerits
Thakur and Juneja [21]	Deep learning-based glaucoma prediction with a CAD system.	To lessen the surgical need for early-stage glaucoma prediction.	Effective minimization of cost.	Training time is very high.
Singh et al. [22]	NB, KNN, ANN and SVM.	To develop an improved deep image model for glaucoma diagnosis.	Localization can be effectively performed.	Consideration of only fewer metrics and a single dataset.
Neto et al. [23]	U-Net based DL architecture	To present a screening of glaucoma in retinal images through the DL framework.	Higher rate of accuracy and robustness.	Analysis can be made only with binary classification.
Cho et al. [24]	CNN	To classify the glaucoma stages using DL- based approach.	Image overfitting can be minimized.	Higher FPR and misprediction rates.
Medeiros et al. [25]	CNN	To assess SD OCT and RNFL thickness variations effectively.	Better distinguishment of progressors can be obtained.	Overall system performance is less.
Jammal et al. [26]	Machine-to-machine algorithm	To compare the ability of machine-to-machine procedure for RNFL thickness evaluation.	Minimization of error and better specificity.	Evaluation outcomes are comparatively less.
Thakur et al. [27]	Glaucoma prediction algorithm	To predict glaucoma from fundus images through a potential longitudinal study.	Better accuracy can be obtained after disease onset.	The degraded similarity of fundus images.
Sejong et al. [28]	Machine learning-based glaucoma prediction approach.	To conduct experiments like RNFL OCT, visual field and IOP for better prediction outcomes.	Effective selection of optimal features can be carried out.	Consumption of time is very high.
Kumar et al. [29]	ResNet-GRU with MDF-HBA	To develop a glaucoma disease detection model to identify the disease changes.	Better accuracy due to optimized parameter tuning	This model has been used in limited training data
Nawaz et al. [30]	Bi-directional Feature Pyramid Network	To effectively identify and classify the glaucomatous regions using accurate optic disc localization	Accurately identified the lesion from distorted images	Fails to identify the important features supported for classification
Kashyap et al. [31]	DenseNet-201 and DCNN	To identify and predict glaucoma disease before symptoms appear	Attained a high level of accuracy due to deep feature extraction	A slight deviation in the classification performance due to improper segmentation
Juneja et al. [32]	Grad-CAM and Modified Xception network	To predict glaucoma at the initial stage through retinal fundus image	Efficient in predicting the earlier stage of glaucoma with less computational complexity	Classification performance has degraded owing to the poor ability of the feature extraction process
Latif et al. [33]	Shallow CNN and pre-trained transfer learning models	To provide accurate glaucoma prediction based on transfer learning	Provides better assistance to ophthalmologists in reducing the burden of mass screening	Certain degradation in accuracy due to overfitting issues

Ibrahim et al.[34]	CNN and artificial algae optimization algorithm	To develop decision support system for Glaucoma disease diagnosis based on deep learning	Robust, accurate and saves computational cost.	Not focused on the segmentation of optic disc and cup

transfer learning based U-Net architecture. Moreover, the pre-trained deep learning model of DenseNet-201 was employed for feature extraction. At last, a deep convolution neural network (DCNN) was used to detect and classify glaucoma disease in retinal fundus images.

Juneja et al. [32] presented a deep learning based glaucoma detection model referred to as classification of glaucoma network (CoG-NET) to exclude the requirement for handcrafted features. Especially, the gradient weighted class activation map (Grad-CAM) is used to analyze regions of interest for disease detection. Finally, modified Xception network based glaucoma classification model is developed with the aid of self-learned significant features.

Latif et al. [33] proposed a two-tier optic disk localization and glaucoma diagnosis network (ODGNet) based on transfer learning-based pre-trained models. In the first tier, the shallow CNN was integrated with a visual saliency map for localizing the optical disk effectively from the fundus images. In the second tier, the pre-trained AlexNet, ResNet, and VGGNet models were used for glaucoma diagnosis. The three pre-trained models follow transfer learning for classifying the extracted optic disc into normal or glaucomatous.

Ibrahim et al. [34] proposed a deep learning based decision support system for glaucoma disease detection. The proposed system comprises two phases; in the first phase, the normalization and mean absolute deviation technique was employed to pre-process the fundus images. In the second phase, the training of the CNN was performed by the artificial algae optimization algorithm. The proposed system achieved good results over other gradient and optimization based deep learning models.

The existing studies have utilized various deep-learning models for glaucoma disease detection. Certain limitations exist in past studies, like improper segmentation, lower capability in extracting useful features, shortage of training data, and attainment of degrading accuracy, which affects the performance of the overall glaucoma disease detection system. The pre-trained deep learning models are efficient for deep feature extraction through self-learning. It takes images as input and creates a model that performs to extract the deep features from those inputted images.

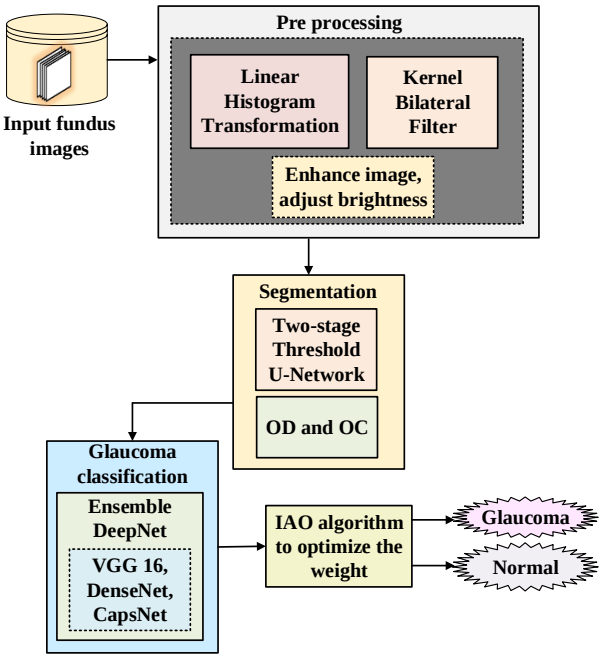

Figure. 1 Automated glaucoma detection framework

However, the ensemble of deep network models is not well studied for glaucoma disease detection. Hence, to conquer these drawbacks and enhance classification accuracy, an Ensemble DeepNet model is proposed in this paper based on the combination of VGGNet, DenseNet, and CapsNet models for accurate glaucoma detection at the early stage.

3. Proposed methodology

Automated glaucoma detection is essential to perform mass screening, even if there is a lack of experienced doctors. This work presents an ensemble deep network (Ensemble DeepNet) for early-stage glaucoma diagnosis using retinal fundus images. However, the analysis uses numerous features to predict glaucoma formation in fundus images. Nowadays, RFI (retinal fundus images) play an important role in the early prediction of glaucoma. The steps used are image acquisition, pre-processing, segmentation, ensemble based deep feature extraction and glaucoma classification.

Initially, retinal fundus images are obtained from the public data source. Pre-processing is necessary to eliminate unwanted image features such as speckles, blind spots etc. The pre-processing steps performed are filtering and linear histogram transformation. The

quality of retinal images is enhanced using the kernel bilateral filter (Kernel BF), eliminating the image noise. Next, the brightness of the input retinal image is adjusted using LHT (linear histogram transformation). The segmentation of OD and OC is performed using a two-stage threshold U-network (Two-stage TUNet). Next, the deep features such as contrast, homogeneity, mean disc, correlation, SD (standard deviation) disc, energy disc, entropy disc, entropy cup, SD cup, mean cup, energy cup, etc., are extracted, and then the glaucoma classification is performed with ensemble DeepNet models such as VGGNet, DenseNet, CapsNet. The loss in the Ensemble DeepNet is optimized using the improved aquila optimization (IAO) algorithm. Moreover, ensemble classification using deep learning is performed for different glaucoma datasets. Fig. 1 shows the early-stage glaucoma disease prediction flow using ensemble optimized deep learning.

3.1 Kernel bilateral filter (Kernel BF)

The detail enhancement filter improves the contrast and visibility features of retinal images. However, it highlights some unpleasant aspects, such as noisy pixels, backdrop roughness, dark shadows, and varying amounts of brightness. Most accessible noise reduction and smoothing filters, such as Gaussian filters, medium and mean, harm image sensitive features, tiny objects, and light edges. A small kernel BF is used to reduce noise and background roughness while precisely preserving the structure of retinal images.

The BF is used in image processing to smoothen, remove noise, and maintain image edges. The Gaussian distribution inserts each pixel value weighted by the related pixels. This filter is used the prior colour detail-enhanced image's grey scale from $(I_{GDE})(I_{DE})$. The bilateral filter equation is as follows:

$$I_{Bil} = \frac{\sum_{o,p} I_{GDE}(o,p)c(q,r,o,p)}{\sum_{o,p} c(q,r,o,p)}, \quad (1)$$

where, I_{Bil} is the image that has been bilaterally filtered, (I_{GDE}) is the image with more detail in the gray scale, q, r are the pixel regions, o and p are the kernel sizes of the filter window, and c denotes normalized weighted value Eq. (2), this is obtained by multiplying the range kernel equation by the domain kernel Eq. (3) and (4).

$$c(q,r,o,p) = exp\left(-\frac{(q-o)^2+(r-p)^2}{2\sigma_x^2} - \frac{f(q-r)+f(o-p)}{2\sigma_x^2}\right) \quad (2)$$

$$x(q,r,o,p) = exp\left(-\frac{(q-o)^2+(r-p)^2}{2\sigma_x^2}\right) \quad (3)$$

$$j(q,r,o,p) = exp\left(-\frac{f(q-r)+f(o-p)}{2\sigma_j^2}\right) \quad (4)$$

where the filter is controlled by the parameters σ_x and σ_j when the range of parameters σ_j rises, the bilateral filter approaches Gaussian blur, whilst increasing domain parameter σ_x promotes smoothness. In this study, the kernel of 3*3 matrixes while σ_x and σ_j are set to 3*3 matrix based on several experiments [35].

3.2 Linear histogram transformation (LHT)

The LHT approach is particularly successful at adjusting the brightness of the input image. When the input image is modified, the intensity is dispersed evenly over the image. The primary goal of this approach is to achieve uniform intensity distribution over the whole image. The cumulative probability function (CDF), defined as the total of all chances in the domain, follows a linear trend, and the discrete transformation equation is as follows:

$$Y_k = X(m_k) = (L-1)\sum_{l=0}^{m} p_m(ml) \quad (5)$$

By assigning an intensity to each pixel in the input image m_k to the parallel pixel Y_k in the output image, the predicted output image is activated, where k is in the range of $[0, L-1]$. The mapping $X(m_k)$ can be referred to as LHT or histogram equalization. The LHT defines the transformation or conversion function that is solely responsible for generating an output image with an identical histogram. Signals are numerous features that are extracted to assure total histograms by characteristics such as contrast, homogeneity, mean disc, correlation, SD (standard deviation) disc, energy disc, entropy disc, entropy cup, SD cup, mean cup, energy cup, and so on [22].

3.3 Segmentation of images

The technique of splitting an image into its component sections using a segment/part of an image is known as image segmentation. The task of the objects is to find a certain sub-division among the provided images. Segmentation is also used in retinal fundus images to investigate structures like the optic disc and optic cup.

3.3.1. OD

The optic nerve head OD is where ganglion cells and axons leave the eye to form the visual cortex. If

there are no shafts or cones, there is a blind zone. Because of the dullness of the receptor rods and cones in that particular region, the corresponding point of the tiny blind spot at the OD is increased. OD is widely employed in the diagnosis of glaucoma to determine the cup-to-disc ratio.

3.3.2. OC

It is located in the middle of the optic disc, which appears to be shaped like a white cup. The optical curve is responsible for the mobility of the retina in the human eye. The greater the distance to the diameter in such an optic curve, the greater the chance of glaucoma.

3.4 Two-stage threshold U-network

The OD and OC are segmented using a two-stage threshold U-network (Two-stage TUNet). During processing, both OD and OC segmentation are two-stage thresholds [29]. A fundamental image processing approach is threshold segmentation. Varying tissues in medical imaging are often displayed at different levels of intensity. The threshold eliminates the uninteresting areas while also reducing noise interference. This process is both required and efficient. The threshold value must be chosen carefully. The region of interest will be impacted if the threshold range is too tiny; as a result, the experimental results are inaccurate. Noise reduction becomes difficult if the threshold range is set too high. The threshold range is often defined by experience. The two-stage U-Net design is used for the threshold interval computations.

Two-stage U-Net: As glaucoma detection must be divided into two groups, it is challenging to segregate glaucoma data in real time (OD and OC). To simplify and reduce the complexity of the problem, a two-stage U-Net framework is used and composed of total glaucoma segmentation (the first stage) and glaucoma substructure segmentation (the second step). Each stage has 2 classification tasks. The primary goal of the second-stage U-net architecture is the segmentation of the many substructures of the system [36]. Fig. 2 illustrates the two-stage U-Net framework.

3.5 Glaucoma classification

The features such as contrast, homogeneity, mean disc, correlation, SD (standard deviation) disc, energy disc, entropy disc, entropy cup, SD cup, mean cup, energy cup, etc., are extracted. Then the Glaucoma classification is performed with Ensemble DeepNet models such as VGGNet, DenseNet, and CapsNet.

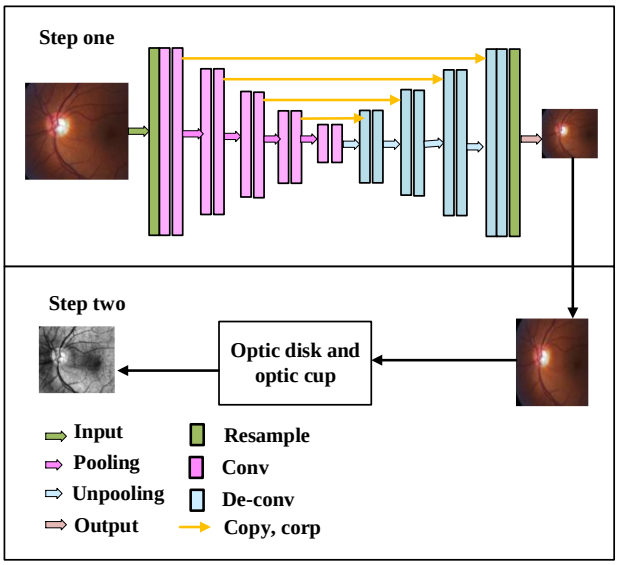

Figure. 2 U-Net framework with two stages

VGGNet, DenseNet, and CapsNet

VGGNet: The VGGNet is a very deep convolutional neural network model, majorly used for image recognition tasks. The image net database was used to train the VGG-16 neural network. Due to the huge training gain of the VGG-16 network, it offers good accuracy even with tiny image datasets. The VGG-16 network has a restricted receptive range and comprises 16 convolution layers of 3×3. There is a maximum pooling layer of size 2×2 and 5 such layers in total. Following the max pooling layer, there are three fully linked layers. As the last layer, it employs the softmax classifier. All hidden layers are activated using ReLu [37].

DenseNet: The DenseNet is a newer DNN with excellent results on various tasks. It is an expanded version of ResNet's successful DNN architecture. In contrast to the ResNet, the DenseNet emphasizes the influence of shortcut connections on subsequent blocks. This exploitation is constructed so that the input image for the coming blocks and the result of the previous blocks is sent to the following blocks. This image has various advantageous qualities, including a reduced vanishing-gradient similar to ResNet, increased feature reuse, and improved feature propagation. Simultaneously, the number of parameters is efficiently reduced [38].

The CapsNet: A better deep network that attempts to represent hierarchical relationships is the capsule network. (CapsNet). CapsNet attempts to imitate biological neuronal structure by retaining hierarchical pose connections. Such a high degree of understanding is difficult since the other networks do not provide this built-in view of an element. The

problem with CapsNet is that it is composed of a collection of neurons whose instantiation parameters are expressed as activity vectors. These vector components provide all necessary information regarding the state of the feature to be detected. The length of an output capsule indicates the possibility that a feature is present in the current input. The directions of the vector also indicate part of the internal state of the examined object.

Recent deep learning research has proposed using an ensemble of DCNNs, which conducts classifications by merging many Deep CNNs to overcome the glaucoma limitations mentioned above. Individual Deep CNN design has diverse visual data recognition capabilities, which assist in increasing the range of the proposed Deep CNN ensemble. In addition, three different types of DCNN were applied (VGGNet, DenseNet, and CapsNet).

A set of M individual DCNNs with no loss were included in the ensemble. Each DCNN's last stage featured a softmax layer, which was followed by a negative log-likelihood layer loss defined as:

$$loss = -\frac{1}{N}\sum_{q=1}^{N} logP_k\left(c_q|x_q^p\right), p \in \{OD, OC\} \quad (6)$$

where, N is the total amount of training data, x_q^p is p^{th} projection of q^{th} training glaucoma data c_q, x_q is the class label of x_q^p, $P_k\left(c_q|x_q^p\right)$ is the posterior probability on the class label c_q for a given x_q^p. It must be noted that a specific projection p was chosen as input for the ensemble's k^{th} Deep CNN.

Moreover, ensemble classification with deep learning is performed for different glaucoma datasets. When training (optimizing) models, a loss function is crucial. It calculates how well the model predicts using a given set of variables. The loss is just a prediction error, and calculating the loss is called the loss function. The loss is 0 if the model's prediction is accurate; otherwise, the loss is greater. An Ensemble DeepNet model was developed to enhance generalized classification to promote interaction and cooperation among Deep CNNs during weight optimization. A loss function is often used in statistics to estimate parameters. The actual event is a function of the difference between estimated and true values for a given data instance. A neural network weight parameter modifies input data inside the network's hidden layers. A neural network is made up of nodes, often known as neurons. Each node has a set of inputs and a weight and bias value.

To utilize the dataset's training portion to compute each configuration's quality using the fitness function shown below. (i.e., it is the root mean

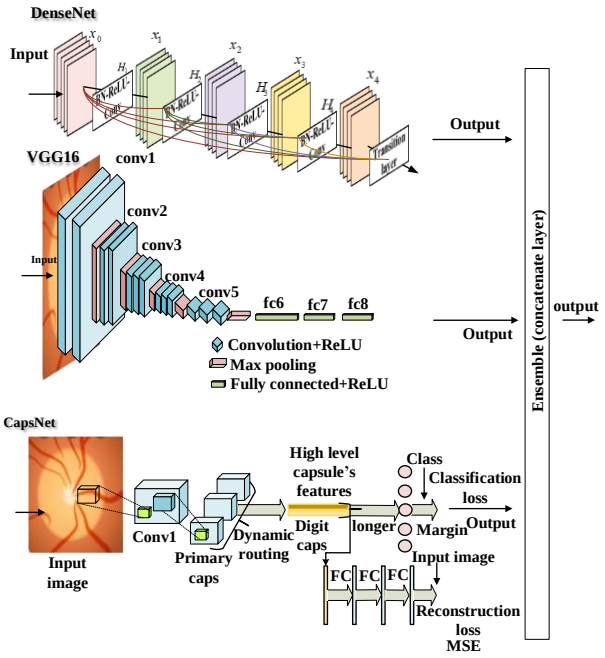

Figure. 3 Block diagram of an ensemble learning model by DenseNet, VGG16, and CapsNet

square error):

$$fit = MSE = \frac{1}{N_y}\sum_{q=1}^{N_g}\left(T_q - P_q\right)^2 \quad (7)$$

where, T and P denotes the actual and predicted output, and the sum of training samples is denoted by N_y. Three modified architectures pre-trained models as depicted in Fig. 3.

Ensemble DeepNet models

3.6 Improved aquila optimizer (IAO)

Aquila's natural hunting behaviour inspired this approach. Based on the benchmarking capabilities of the statistical results, the admirably performed AO algorithm finds the best solution. However, in other traditional optimization procedures, the exploration and exploitation capabilities of the AO algorithm can still be improved. The primary idea behind enhanced algorithms is to improve accuracy and keep the balance between global search and local exploitation capabilities used to avoid premature convergence and increase convergence speed. Consequently, the original AO algorithm was enhanced with two improvement procedures [39].

Random initialization is used to produce the initial population of weight X. The formal expression is as follows:

$$X_{qr} = LB_r + rand \times (UB_r - LB_r), \quad q = 1,2,\ldots..,P, r = 1,2,\ldots..,D \quad (8)$$

where, X indicates a set of current x solutions randomly created $rand$ is a random number between 0 and 1, P indicates the population size, and D denotes the problem dimension. The upper and lower limits of the search agent in the r^{th} dimension search space is represented by UB_r and LB_r, respectively.

Here, x identifies and selects the optimal location X by conducting a soaring high stooping vertically (X_1). The AO investigates the search sector for the best location X from a great height. This process is mathematically indicated as Eq. (9).

$$X_1(t+1) = X_{best}(t) \times \left(1 - \frac{t}{T}\right) + (X_M(t) - X_{best}(t) \times rand) \quad (9)$$

where, $X_1(t+1)$ is the next iteration's solution of t created. $X_{best}(t)$ is the most useful key found until t^{th} iteration, it depicts the approximate position optimal X. $\left(1 - \frac{t}{T}\right)$ is employed to limit the number of iterations in the extended investigation. $X_M(t)$ is the average of all current solutions during t^{th} iteration, as computed by Eq. (10). $rand$ is a number between 0 and 1. The current number of iterations is t, and the maximum number of iterations is T.

$$X_M(t) = \frac{1}{P}\sum_{q=1}^{P} X_q(t), \forall r = 1,2, \dots \dots, D \quad (10)$$

where, D the problem of dimension and P is the population number.

Here, the optimal X is discovered using Aquila's contour flying method with a short glide. The Aquila circles over intended prey to catch its prey; likewise, the optimal X can also be detected and is mathematically expressed as,

$$X_2(t+1) = X_{best}(t) \times levy(D_s) + X_{Ra}(t) + (y - x) \times rand \quad (11)$$

where, $X_2(t+1)$ indicates the next iteration t created, i.e. X_2 , D_s denotes the dimensional space, $levy(D_s)$ represents the levy for the flight distribution function, and Eq. (12) is used. In the t^{th} iteration, $X_{Ra}(t)$ is a random solution picked from N solution.

$$levy(D_s) = c \times \frac{u \times \sigma}{|v|^{\frac{1}{\beta}}} \quad (12)$$

where c is an updated constant of 0.01, u and v are random values between 0 and 1.

The following formula is used to calculate σ value:

$$\sigma = \left(\frac{\gamma(1+\beta) \times sin\left(\frac{\pi\beta}{2}\right)}{\gamma\left(\frac{1+\beta}{2}\right) \times \beta \times 2^{\frac{\beta-1}{2}}}\right) \quad (13)$$

where σ is a fixed constant value of 1.5, the spiral from the process is represented by γ and β in Eq. (11), and the equation:

$$y = r \times cos(\theta), x = r \times sin(\theta) \quad (14)$$

$$r = r_1 + F \times I_1 \quad (15)$$

$$\theta = -\omega \times I_1 + \theta_1 \quad (16)$$

$$\theta_1 = \frac{3 \times \pi}{2} \quad (17)$$

where, r_1 set the count of search cycles, enter a value between 1 and 20, and F is a constant of 0.00565. I_1 positive numeral between 1 and the length of the search space (I), and ω is a permanent value of 0.005.

Here, X is accurately identified by using the technique of low flying of aquila with a slow descent attack (X_3). The aquila is prepared to land and begins its descent with a preliminary attack vertically to identify its target. Likewise, the optimal X can also be detected and is mathematically expressed as,

$$X_3(t+1) = (X_{best}(t) - X_M(t)) \times \alpha - rand + \left((UB - LB) \times rand + LB\right) \times \delta \quad (18)$$

where, $X_3(t+1)$ are the results of the third search method's following iteration of t, $X_{best}(t)$ represents the approximate location of the optimal X after the i^{th} iteration (optimal value) and $X_M(t)$ shows the present solution's mean value at the t^{th} iteration, as driven by Eq. (10). $rand$ is a number chosen at random between 0 and 1. α and δ are exploitation adjustment variables that have been set at 0.1. UB and LB the problem's upper and lower limits, respectively

Here, X is identified based on its stochastic motions using the fourth technique (X_4) walk around and catch prey. The aquila goes for a walk and grabs its prey; likewise, the optimal can also be detected and is mathematically expressed as,

$$X_4(t+1) = QuF \times X_{best}(t) - (V_1 \times X(t) \times rand) - V_2 \times loss(D) + rand \times V_1 \quad (19)$$

where, $X_4(t+1)$ represents the solution obtained by the next iteration of t is generated by (X_4). QuF is optimize the search technique, the

quality function is applied, and it is determined using Eq. (20). V_1 is the Aquila tracking prey's varied motions, created using Eq. (21). V_1 indicates that Eq. (22) produces a decreasing number from 2 to 0. The currently available solution in the t^{th} iteration is $X(t)$.

$$QuF(t) = t^{\frac{2\times rand-1}{(1-T)^2}} \quad (20)$$

$$V_1 = 2 \times rand - 1 \quad (21)$$

$$V_2 = 2 \times \left(1 - \frac{t}{T}\right) \quad (22)$$

where, $QuF(t)$ is the quality function's value in the t^{th} iteration and $rand$ is a random number between 0 and 1.

The IAO algorithm is finally executed to find the best set of weights for three pre-trained deep learning networks to minimize the classification error of the ensemble model. The weights of models normalized between 0 and 1, inclusive, and their sum will be 1.

4. Result and discussion

The experimental setup, performance measurement, evaluation datasets, and experimental outcomes are all described in this section. The discussion of the results includes an evaluation of the proposed Ensemble DeepNet model. The parameters of accuracy, precision, sensitivity and specificity are used to evaluate the performance of the proposed model with the existing models.

4.1 Dataset description

The experiment was based on rim-one-dl and kaggle glaucoma detection (KGD). The total number of images in the kaggle data set is 12482. Kaggle dataset gives glaucoma negative images 386, glaucoma positive images 134 for training, and for testing glaucoma negative images 96, and glaucoma positive images 34.

Rim-one-dl: Some confusion and incorrect usage of the three published versions prompted the proposal to update and integrate them into a new version named Rim-one DL (rim one for deep learning). It is optimized for a deep-learning environment by the previously mentioned standards. The outcome of integrating the three previous versions is rim-one DL. This gives each patient and each eye a separate image. In addition, all images were properly cropped around the head of the optic nerve using the same proportionality criterion, which had not been done in previous iterations. Here the total number of images taken is 12139.

Table 2. Simulation parameters of both datasets.

Simulation parameters for KGDand Rim-one-dl	Values
Batch_size	2
Epoch	100
Input size	128, 128, 3
Activation function	Sigmoid
Dropout	0.5
Kernel size	(3,3)

4.2 Simulation environment

Evaluate the proposed early-stage glaucoma disease prediction technique using the python software in a simulated environment utilizing rim-one-dl and KGD datasets. The test is run on a machine equipped with an Intel(R) Core(TM) i5-3470 CPU @ 3.20GHz, 3200 Mhz, 4 core(s), 4 logical pro. And micro software 10 pro, a micro soft corporation, is an OS manufacturer installed physical memory (RAM) 8GM. The table below shows the simulation parameters of the KGD dataset and the rim-one-dl dataset. Table 2 shows simulation parameters for the rim-one-dl and KGD datasets.

4.3 Visual representation of rim-one-dl and KGD datasets

The OD and OC use a two-stage threshold U-network (Two-stage TUNet). A glaucoma patient is larger than a typical person. Figs. 4 and 5 depict typical fundus images from both categories and the sample from one position from the dataset's optic disc and cup area of the rim-one-dl, KGD datasets.

Below, Table 3 shows the segmentation values of parameters for both datasets. Since it extracts the items of interest for additional processing, such as description or identification, segmentation is a key stage of the image recognition system. Image segmentation is used in practice to classify image pixels.

5. Performance evaluation

A confusion matrix is a table that describes the performance of a classification model (or classifier) on a set of test data with known true values. The confusion matrix is easy to understand, but the vocabulary can be difficult. Fig. 6 depicts the confusion matrix for both datasets.

Sensitivity, specificity, accuracy and recall are tested for performance evaluation. This proposed model was found to have individual implications for

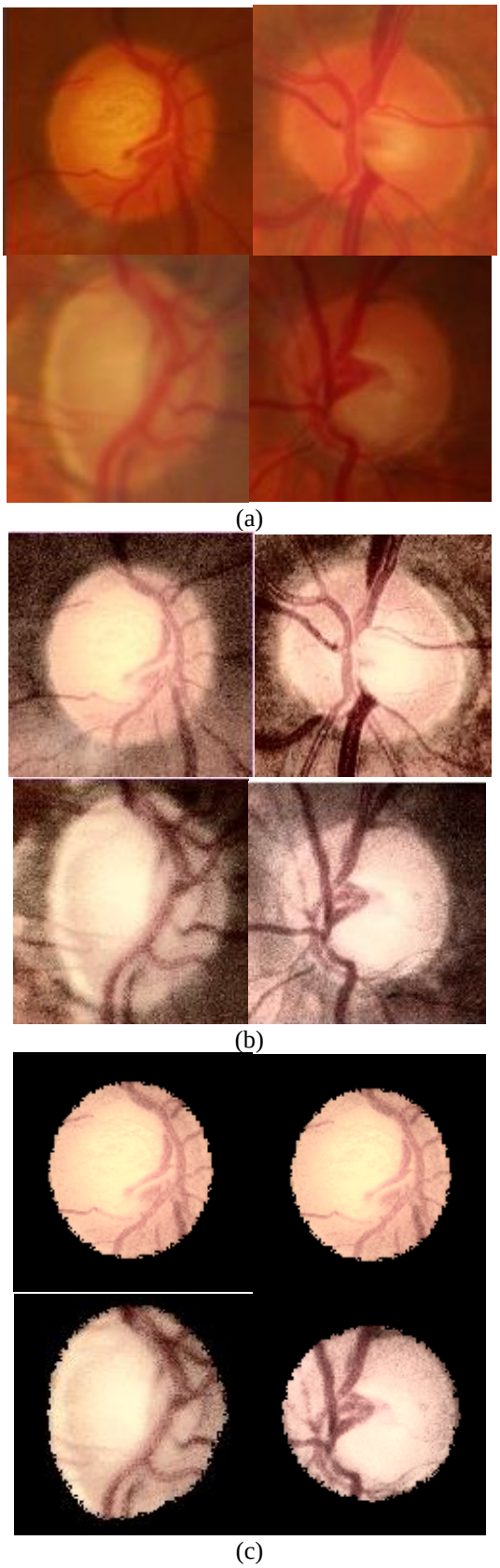

(a) (b) (c)

Figure. 4 Visual representation of normal and glaucoma images from the rim-one-dl dataset: (a) Source image, (b) Pre-processed image, and (c) Segmented image

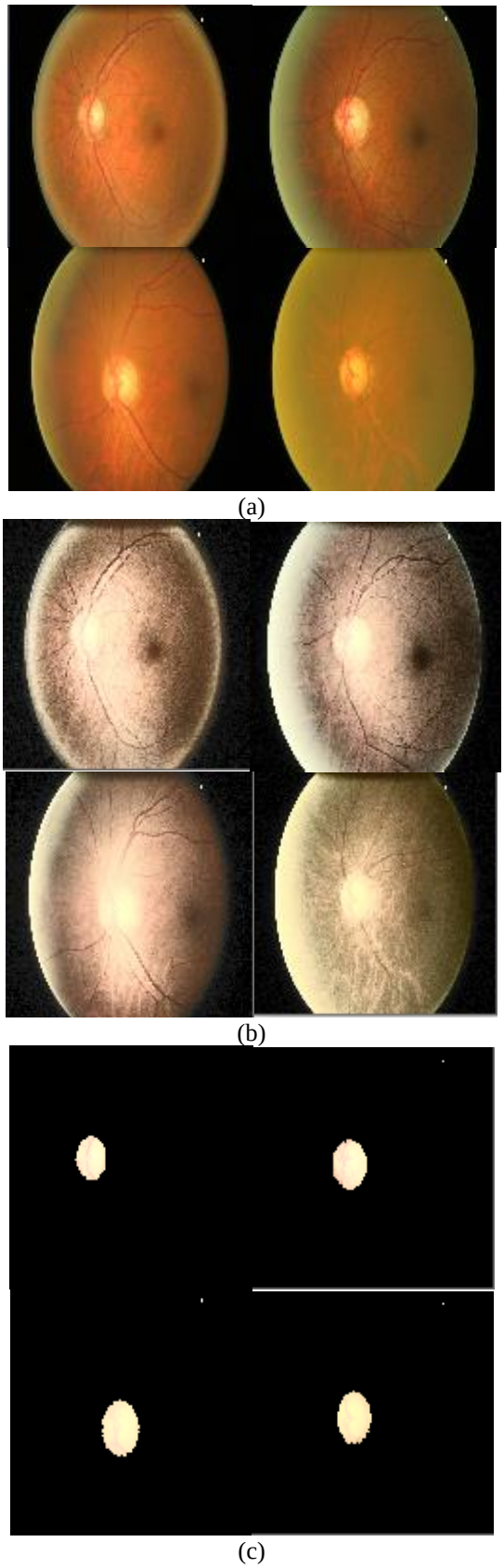

(a) (b) (c)

Figure. 5 Visual representation of normal and glaucoma images from the KGD dataset: (a) Source image, (b) Pre-processed image, and (c) Segmented image

Table 3. Segmentation values for both datasets

Parameters	Rim-one-dl	KGD
Accuracy	97%	97%
Recall	95%	95%
Precision	99%	99%
F1 Score	97%	97%
Jaccard index	95%	95%
Dice index	97%	97%
RMSE	18%	18%
SSIM	99%	100%

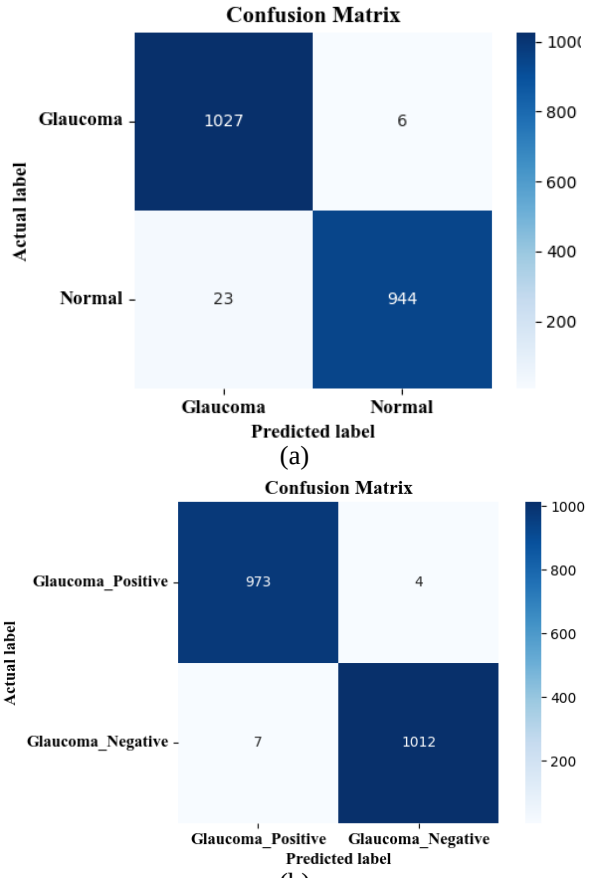

Figure. 6 Confusion matrix: (a) rim-one-dl dataset and (b) KGD dataset

different existing techniques for the two data sets, rim-one-dl and KGD.

5.1 Comparative analysis

The plot of CapsNet, Figs. 7 (a), and 8 (a) show a larger difference between validation and training accuracy. This shows that the model may be overfitted. Furthermore, the improvement in accuracy has not been constant. There are substantial gaps between training and validation at a few epochs. Furthermore, at the last epoch, the training accuracy is significantly lower than the validation accuracy.

Furthermore, in the DenseNet plots in Figs. 7 (b) and 8 (b), the training accuracy is higher than the validation accuracy. This indicates that the model is overfitting, and the peaks are not increasing consistently. The training accuracy of DenseNet is continually rising, however, the validation accuracy is not. There is also a decrease in validation accuracy after a few epochs, which is undesirable. As a result, the model underperforms and is unsuitable for predicting abnormality. In the case of VGG 16, Figs. 7 (c), and 8 (c), the training and validation curves follow a similar pattern. Figs. 7 and 8 show the epoch vs. Loss plot for ensemble DeepNet for the rim-one-dl and KGD datasets. Fig. 9 shows the overall performance of the rim-one-dl dataset, the KGD dataset.

Epoch: An epoch in artificial neural networks is one loop that covers the whole training dataset. Training a neural network typically takes many epochs.

Loss: The loss is the mean error over the training data after each epoch.

Figs. 7 and 8 depict the epoch and loss values for the training and testing time processes of the caps net, dense net, and VGG16.

Fig. 9 depicts the overall performance of several criteria, such as accuracy, specificity, recall, and precision, using the rim-one-dl and KGD datasets. It is based on deepnet ensembles such as caps net, dense net, and VGG16. The final classification result is the overall performance.

ROC curves were displayed to visually evaluate ensemble approaches based on the association between true positive and false positive rates for each deepNet. Figure 10 shows better outcomes when such a curve is closer to the top-left corner. Using the rim-one-dl and KGD datasets, the AUC value outperforms the existing Deepnet CapsNet, DenseNet, and VGG16. The proposed AUC for the rim-one-dl dataset is 0.985, while the AUCs for the caps net, dense net, and VGG net are 0.964, 0.961, and 0.956, respectively. The AUC proposed in the KGD dataset was 0.994, while caps net, dense net, and VGG net AUCs were 0.993, 0.991, and 0.991, respectively. The ROC curve depicts the relationship between sensitivity (and TPR) and specificity (1 - FPR). As a baseline, a random classifier is expected to give points along the diagonal (FPR = TPR).

Table 4 presents the comparison of some of the existing methods and proposed models in terms of accuracy, precision and recall. Table 4 indicates that the two existing methods have good accuracy and recall performance [30, 33]. The proposed model is more efficient in accuracy and recall for glaucoma disease detection. The above comparison table

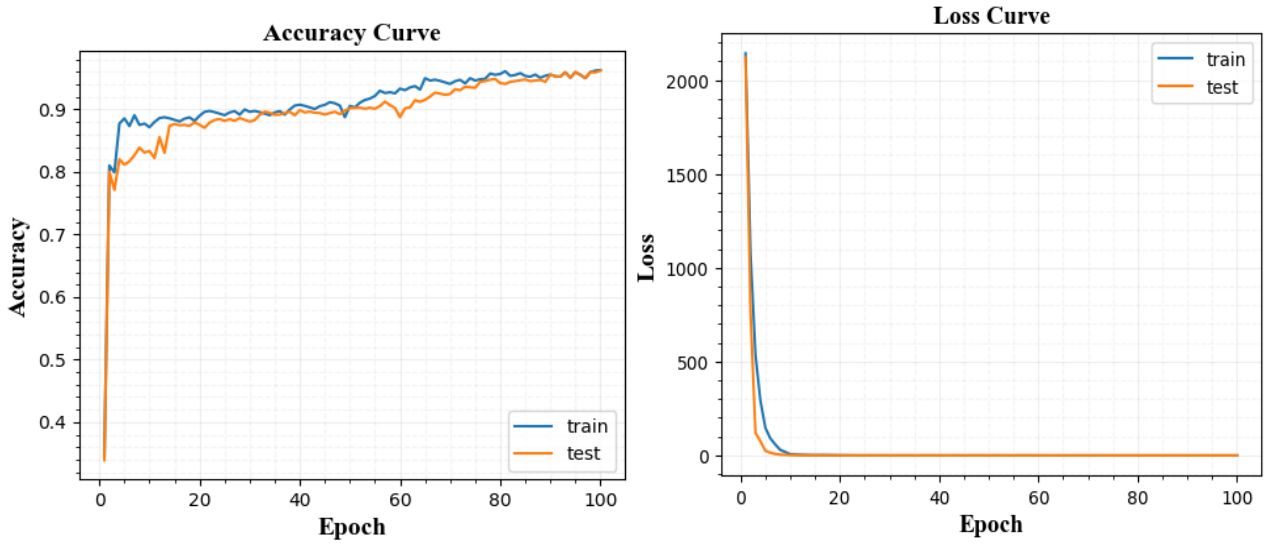

(a)

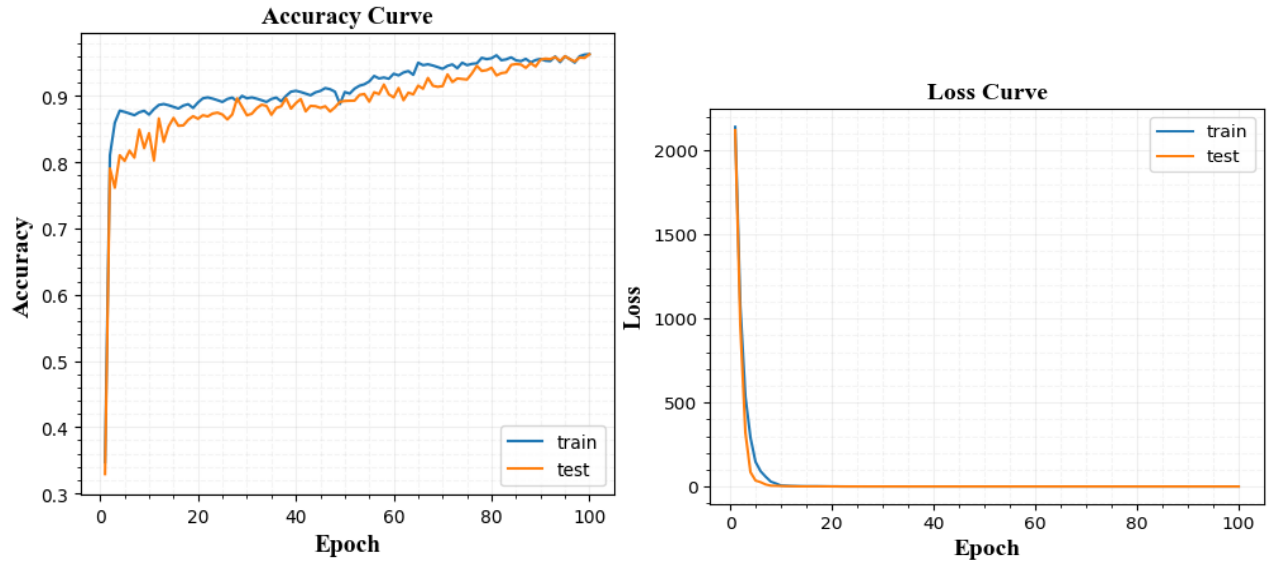

(b)

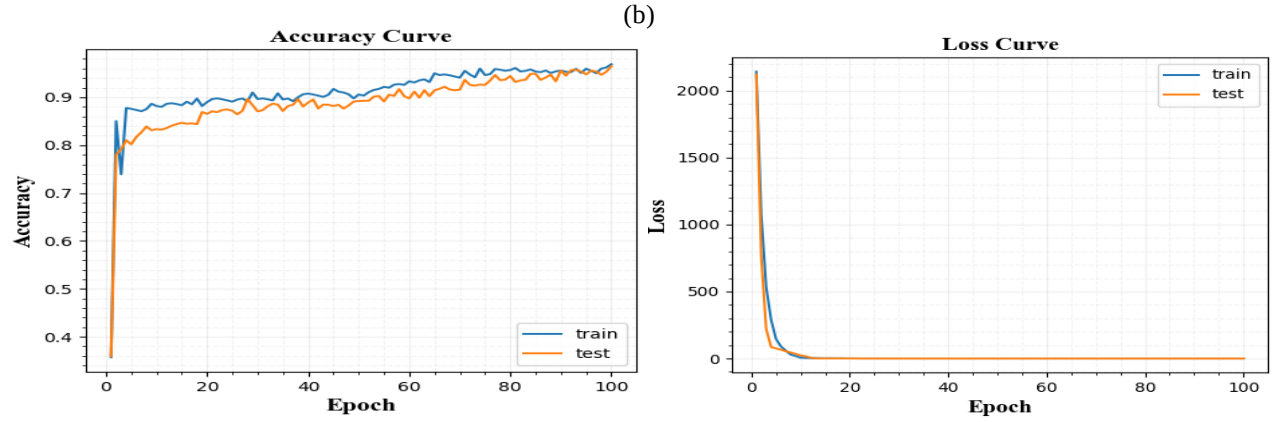

(c)

Figure. 7 Epoch vs. Loss plot in ensemble DeepNet for the rim-one-dl dataset: (a) Epoch vs. loss for caps net, (b) Epoch vs. loss for densenet, and (c) Epoch vs. loss for VGG16

indicates that some existing methods are less efficient in performance in terms of accuracy and precision [21, 23]. Moreover, certain existing methods are moderately efficient but still suffer in performance in terms of accuracy and precision [29, 31]. But the proposed model achieved better detection performance in predicting glaucoma disease in the early stage.

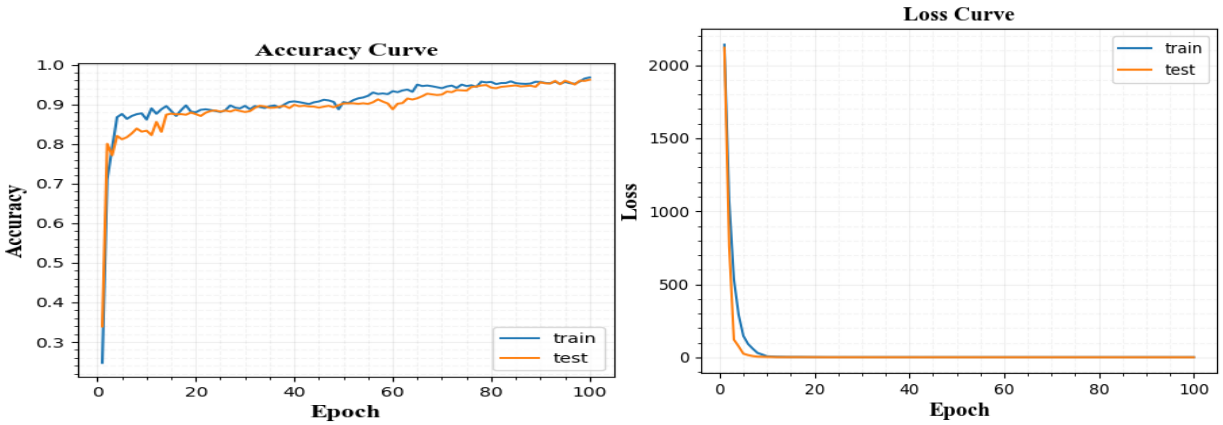

(a)

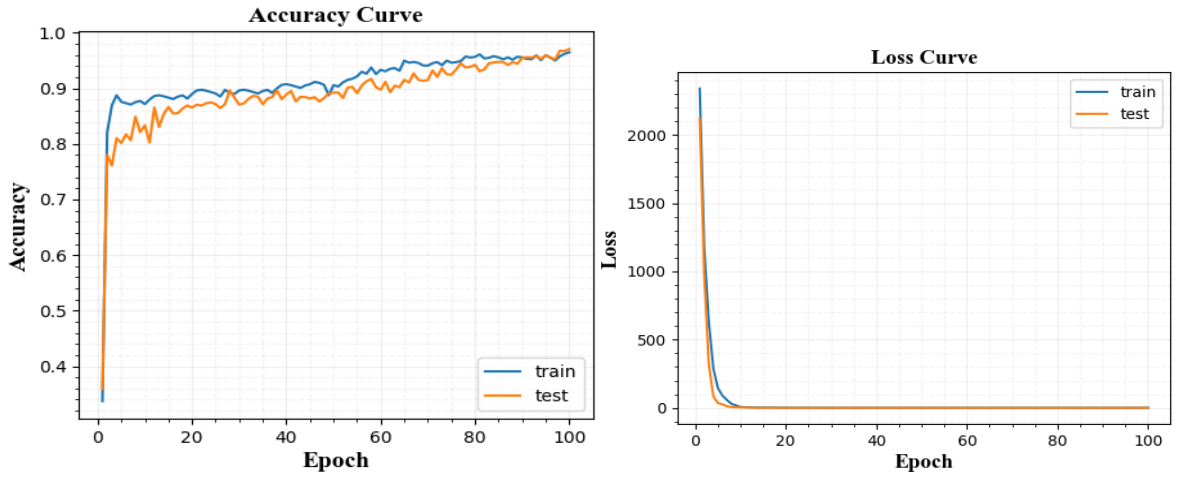

(b)

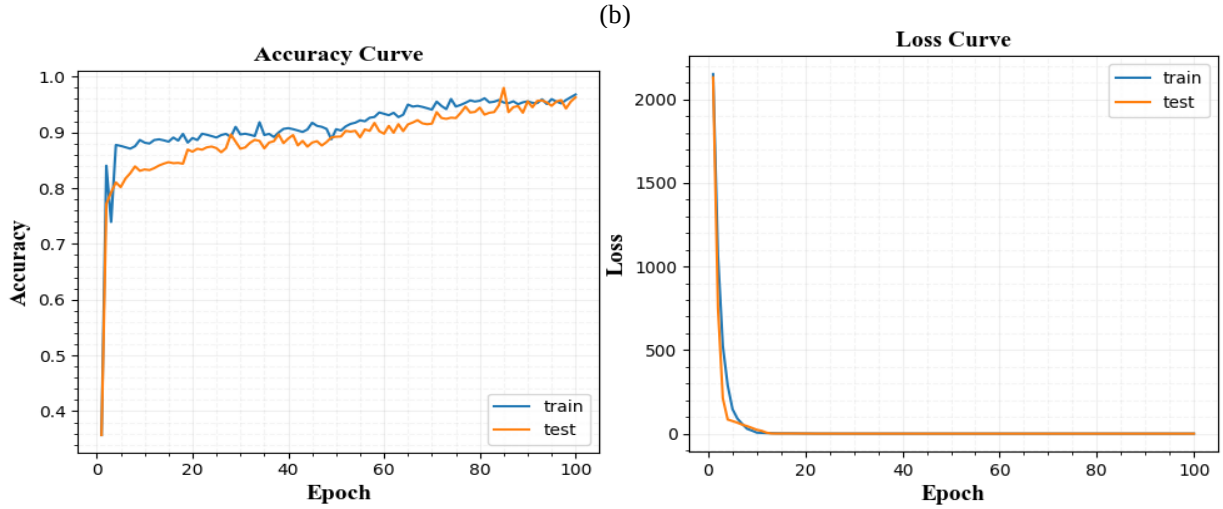

(c)

Figure. 8 Epoch vs. loss in ensemble DeepNet for KGD dataset: (a) Epoch vs. loss for caps net, (b) Epoch vs. loss for densenet, and (c) Epoch vs. loss for VGG16

6. Conclusions

Doctors can make a more accurate diagnosis in less time by using image processing tools to detect glaucoma early. This study provides an ensemble deep network (Ensemble DeepNet) model for early-stage glaucoma detection using retinal fundus images. Traditional retinal imaging techniques are either less automated or less accurate. This paper aims to design and develop an accurate automated glaucoma diagnostic system for anomaly classification. The proposed image feature-based model assists medical practitioners in diagnosing the existence of glaucoma with more precision and less calculation time. It has been discovered that retrieved characteristics are interdependent and must be merged to construct

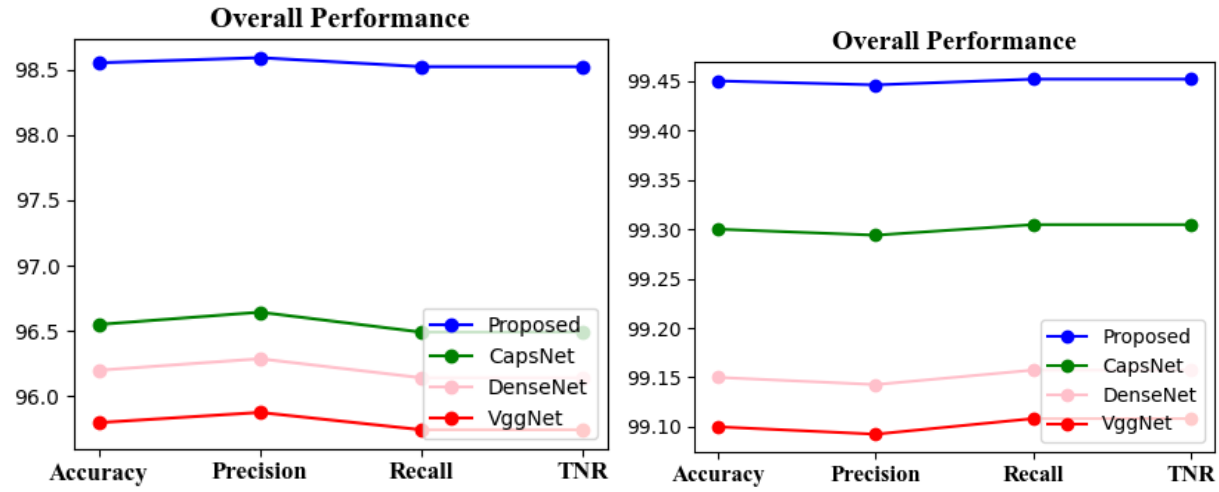

Figure. 9 Overall performance of both datasets

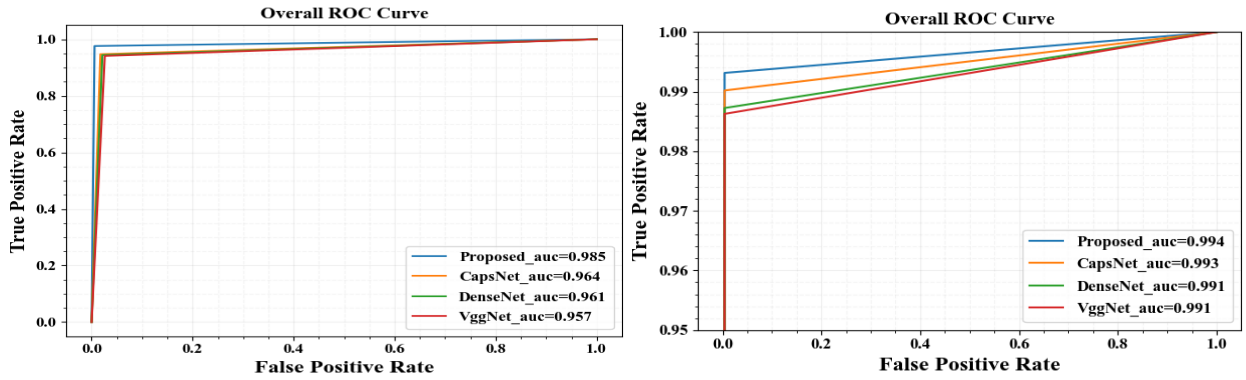

(a) (b)

Figure. 10 ROC curves of ensemble methods using CapsNet, DenseNet, and VGG16: (a) rim-one-dl dataset and (b) KGD dataset

Table 4. Comparison with the existing method

Method	Accuracy (%)	Precision (%)	Recall (%)
Proposed	99.45	99.45	99.45
XceptionNet [21]	93.1	90.1	91.8
Inception ResNet V2 [23]	95	83	96
ResNet-GRU [29]	96.46	90.5	96.43
BiFPN [30]	97.96	-	97
DenseNet-201 [31]	96.45	-	97.03
Modified XceptionNet [32]	95.3	-	95
Shallow CNN and transfer learning [33]	95.75	-	94.75
Optimized CNN	98.15	-	97.95

parameter-based inquiry for glaucoma in the retinal fundus. The accuracy value for the proposed method of the rim-one-dl dataset is 97.7%, and the KGD dataset values are 99.45%, respectively.

Conflicts of interest

The authors declare no conflict of interest.

Author contributions

Jincy C Mathew - Conceptualization, methodology, software, formal analysis, investigation, data curation, writing—original draft preparation,

V. Ilango - writing—review and editing, visualization, supervision, project administration.

V. Asha - validation, resources, review and editing, visualization,

References

[1] X. Zhang, S. Vadoothker, W. Munir, and O. Saeedi, "Ocular Surface Disease and Glaucoma Medications: A Clinical Approach", *Eye &; Contact Lens: Science & Clinical Practice*, Vol. 45, pp. 11-18, 2019.

[2] T. Chan, C. Bala, A. Siu, F. Wan, and A. White, "Risk Factors for Rapid Glaucoma Disease

Progression", *American Journal of Ophthalmology,* Vol. 180, pp. 151-157, 2017.

[3] H. Springelkamp, A. I. Iglesias, A. Mishra, R. Höhn, R. Wojciechowski, A. P. Khawaja, A. Nag, Y. X. Wang, J. J. Wang, G. C. Partida, and J. Gibson, "New insights into the genetics of primary open-angle glaucoma based on meta-analyses of intraocular pressure and optic disc characteristics", *Human Molecular Genetics,* Vol. 26, No. 2, pp. 438-53, 2017.

[4] H. Quigley, "The number of people with glaucoma worldwide in 2010 and 2020", *British Journal of Ophthalmology,* Vol. 90, pp. 262-267, 2006.

[5] L. Fry, E. Fahy, V. Chrysostomou, F. Hui, J. Tang, and P. V. Wijngaarden, "The coma in glaucoma: Retinal ganglion cell dysfunction and recovery", *Progress in Retinal and Eye Research,* Vol. 65, pp. 77-92, 2018.

[6] Y. Jung, K. Han, S. Wang, H. Yoon, and J. Moon, "Effect of depressive symptom and depressive disorder on glaucoma incidence in elderly", *Scientific Reports,* Vol. 11, 2021.

[7] S. Berchuck, S. Hunt, A. Shi, G. Singh, A. A. Jammal, and F. A. Medeiros, "Identifying risk factors for blindness from glaucoma at first presentation to a tertiary clinic", *Investigative Ophthalmology & Visual Science,* Vol. 62, No. 8, p. 1588, 2021.

[8] J. Stein, A. Khawaja, and J. Weizer, "Glaucoma in Adults—Screening, Diagnosis, and Management", *JAMA,* Vol. 325, p. 164, 2021.

[9] S. Chakrabarty, S. Chandrashekharan, M. Tanwar, B. Madhuvarasu, M. Uduman, and R. Ramakrishnan, "Outcomes and favourable prognostic factors in patients of phacomorphic and phacolytic glaucoma managed by manual small-incision cataract surgery: A retrospective study", *Indian Journal of Ophthalmology,* Vol. 70, p. 1216, 2022.

[10] S. Maheshwari, "Advanced image analysis techniques for automated glaucoma diagnosis using retinal fundus images", *Manakin Repository,* 2020, http://dspace.iiti.ac.in:8080/jspui/handle/123456789/2491

[11] J. Wang, Z. Wang, F. Li, G. Qu, Y. Qiao, and H. Lv, "Joint retina segmentation and classification for early glaucoma diagnosis", *Biomedical Optics Express,* Vol. 10, p. 2639, 2019.

[12] Y. Hagiwara, J. Koh, J. Tan, S. Bhandary, A. Laude, and E. Ciaccio, "Computer-aided diagnosis of glaucoma using fundus images: A review", *Computer Methods and Programs in Biomedicine*, Vol. 165, pp. 1-12, 2018.

[13] L. A. Hamid, "TWEEC: Computer-aided glaucoma diagnosis from retinal images using deep learning techniques", *International Journal of Imaging Systems and Technology*, Vol. 32, pp. 387-401, 2021.

[14] M. Tanito, K. Sugihara, K. Hara, and Y. Takai, "Different glaucoma types and glaucoma surgeries among different age groups", *Graefe's Archive for Clinical and Experimental Ophthalmology*, Vol. 256, pp. 2013-2014, 2018.

[15] J. Myers, S. Fudemberg, and D. Lee, "Evolution of optic nerve photography for glaucoma screening: a review", *Clinical & Amp; Experimental Ophthalmology*, Vol. 46, pp. 169-176, 2018.

[16] H. Veena, A. Muruganandham, and T. Kumaran, "A Review on the optic disc and optic cup segmentation and classification approaches over retinal fundus images for detection of glaucoma", *SN Applied Sciences,* Vol. 2, 2020.

[17] H. Almubarak, Y. Bazi, and N. Alajlan, "Two-Stage Mask-RCNN Approach for Detecting and Segmenting the Optic Nerve Head", *Optic Disc, and Optic Cup in Fundus Images, Applied Sciences,* Vol. 10, p. 3833, 2020.

[18] G. An, K. Omodaka, K. Hashimoto, S. Tsuda, Y. Shiga, and N. Takada, "Glaucoma Diagnosis with Machine Learning Based on Optical Coherence Tomography and Color Fundus Images", *Journal of Healthcare Engineering,* Vol. 2019, pp. 1-9, 2019.

[19] G. Lim, Y. Cheng, W. Hsu, and M. L. Lee, "Integrated optic disc and cup segmentation with deep learning", In: *Proc. of 2015 IEEE 27th International Conference on Tools with Artificial Intelligence (ICTAI)*, pp. 162-169, 2015.

[20] Y. Chai, H. Liu, and J. Xu, "Glaucoma diagnosis based on both hidden features and domain knowledge through deep learning models", *Knowledge-Based Systems,* Vol. 161, pp. 147-156, 2018.

[21] N. Thakur and M. Juneja, "Early-stage prediction of glaucoma disease to reduce surgical requirements using deep-learning", *Materials Today: Proceedings,* Vol. 45, pp. 5660-5664, 2021.

[22] L. Singh, Pooja, H. Garg, M. Khanna, R. Bhadoria, "An enhanced deep image model for glaucoma diagnosis using feature-based detection in retinal fundus", *Medical & Biological Engineering & Computing*, Vol. 59, pp. 333-353, 2021.

[23] A. Neto, J. Camara, and A. Cunha, "Evaluations of Deep Learning Approaches for Glaucoma

Screening Using Retinal Images from Mobile Device", *Sensors*, Vol. 22, p. 1449, 2022.
[24] H. Cho, Y. Hwang, J. Chung, K. Lee, J. Park, and H. Kim, "Deep Learning Ensemble Method for Classifying Glaucoma Stages Using Fundus Photographs and Convolutional Neural Networks", *Current Eye Research*, Vol. 46, pp. 1516-1524, 2021.
[25] F. Medeiros, A. Jammal, and E. Mariottoni, "Detection of Progressive Glaucomatous Optic Nerve Damage on Fundus Photographs with Deep Learning", *Ophthalmology*, Vol. 128, pp. 383-392, 2021.
[26] A. Jammal, A. Thompson, E. Mariottoni, S. Berchuck, C. Urata, and T. Estrela, "Human Versus Machine: Comparing a Deep Learning Algorithm to Human Gradings for Detecting Glaucoma on Fundus Photographs", *American Journal Of Ophthalmology*, Vol. 211, pp. 123-131, 2020.
[27] [27] A. Thakur, M. Goldbaum, S. Yousefi, "Predicting Glaucoma before Onset Using Deep Learning", *Ophthalmology Glaucoma*, Vol. 3, pp. 262-268, 2020.
[28] S. Oh, Y. Park, K. Cho, and S. Kim, "Explainable Machine Learning Model for Glaucoma Diagnosis and Its Interpretation", *Diagnostics*, Vol. 11, p. 510, 2021.
[29] V. V. Kumar, G. H. Reddy, and M. N. G. Prasad, "A novel glaucoma detection model using Unet++-based segmentation and ResNet with GRU-based optimized deep learning", *Biomedical Signal Processing and Control*, Vol. 86, p. 105069, 2023.
[30] M. Nawaz, T. Nazir, A. Javed, U. Tariq, H. S. Yong, M. A. Khan, and J. Cha, "An efficient deep learning approach to automatic glaucoma detection using optic disc and optic cup localization", *Sensors*, Vol. 22, No. 2, p. 434, 2022.
[31] R. Kashyap, R. Nair, S. M. Gangadharan, M. B. Tobar, S. Farooq, and A. Rizwan, "Glaucoma detection and classification using improved U-Net Deep Learning Model", *Healthcare*, Vol. 10, No. 12, p. 2497, 2022.
[32] M. Juneja, S. Thakur, A. Uniyal, A. Wani, N. Thakur, and P. Jindal, "Deep learning-based classification network for glaucoma in retinal images", *Computers and Electrical Engineering*, Vol. 101, p. 108009, 2022.
[33] J. Latif, S. Tu, C. Xiao, S. U. Rehman, A. Imran, and Y. Latif, "ODGNet: a deep learning model for automated optic disc localization and glaucoma classification using fundus images", *SN Applied Sciences*, Vol. 4, No. 4, p. 98, 2022.
[34] M. H. Ibrahim, M. Hacibeyoglu, A. Agaoglu, and F. Ucar, "Glaucoma disease diagnosis with an artificial algae-based deep learning algorithm", *Medical & Biological Engineering & Computing*, Vol. 60, No. 3, pp. 785-796, 2022.
[35] B. Bataineh and K. Almotairi, "Enhancement Method for Color Retinal Fundus Images Based on Structural Details and Illumination Improvements", *Arabian Journal for Science And Engineering*, Vol. 46, pp. 8121-8135, 2021.
[36] T. Liu, Y. Tian, S. Zhao, X. Huang, and Q. Wang, "Automatic Whole Heart Segmentation Using a Two-Stage U-Net Framework and an Adaptive Threshold Window", *IEEE Access*, Vol. 7, pp. 83628-83636, 2019.
[37] D. Theckedath and R. Sedamkar, "Detecting Affect States Using VGG16, ResNet50 and SE-ResNet50 Networks", *SN Computer Science*, Vol. 1, 2020.
[38] M. Javidi, S. Abbaasi, S. N. Atashi, and M. Jampour, "COVID-19 early detection for imbalanced or low number of data using a regularized cost-sensitive CapsNet", *Scientific Reports*, Vol. 11, 2021.
[39] L. Ma, J. Li, and Y. Zhao, "Population Forecast of China's Rural Community Based on CFANGBM and Improved Aquila Optimizer Algorithm", *Fractal and Fractional*, Vol. 5, p. 190, 2021.

Nomenclature

Symbols	Explanations
I_{Bil}	bilaterally filtered image
I_{GDE}	image with more detail in the gray scale
q, r	pixel regions
o, p	kernel sizes
m_k	each pixel in the input image
Y_k	parallel pixel
N	total amount of training data
$c_q,\ x_q$	class label
$P_k(c_q \mid x_q^p)$	posterior probability on the class label
T	actual output
P	predicted output
N_y	training samples
$rand$	random number

UB_r	upper limit of the search agent
LB_r	lower limit of the search agent
D	dimension
D_s	dimensional space
c	updated constant
σ	fixed constant
I	length of the search space
α, δ	exploitation adjustment variables
QuF	quality function